**Proceedings of ASME Turbo Expo 2011**
**GT2011**
**June 6-10, 2011, Vancouver, British Columbia, Canada**

# GT2011-45266

## A NEW, ITERATIVE, SYNCHRONOUS-RESPONSE ALGORITHM FOR ANALYZING THE MORTON EFFECT

**Dara W. Childs**
Turbomachinery Laboratory,
Texas A&M University,
College Station, TX 77843 USA
**dchilds@tamu.edu**

**Rohit Saha**
Graduate Research Assistant
Texas A&M University
College Station, TX 77845
**saha.rohit@gmail.com**

## ABSTRACT

Morton Effect problems involve the steady increase in rotor synchronous-response amplitudes due to differential heating across a fluid-film bearing that is in turn induced by synchronous response. The present work presents a new computational algorithm for analyzing Morton Effect. Previous studies on the Morton Effect were based on Eigen or Nyquist analysis for stability studies and predicted an onset speed of instability.

The algorithm starts with a steady state elliptical orbit produced by the initial imbalance distribution, which is decomposed into a forward-precessing circular orbit and a backwards-precessing circular orbit. A separate (and numerically intensive) calculation based on the Reynolds equation plus the energy equation gives predictions for the temperature distributions induced by these separate orbits for a range of orbit radius-to-clearance ratios. Temperature distributions for the forward and backward orbits are calculated and added to produce the net temperature distribution due to the initial elliptic orbit. The temperature distribution is assumed to vary linearly across the bearing and produces a bent-shaft angle across the bearing following an analytical result due to Dimoragonas. This bent shaft angle produces a synchronous rotor excitation in the form of equal and opposite moments acting at the bearing's ends. For a rotor with an overhung section, the bend also produces a thermally induced imbalance. The response due to the initial mechanical imbalance, the bent-shaft excitation, and the thermally-induced imbalance are added to produce a new elliptic orbit, and the process is repeated until a converged orbit is produced. For the work reported, no formal stability analysis is carried out on the converged orbit.

The algorithm predicts synchronous response for the speed range of concern plus the speed where the response amplitudes becomes divergent by approaching the clearance.

Predictions are presented for one examples from the published literature, and elevated vibration levels are predicted well before the motion diverges. Synchronous-response amplitudes due to Morton Effect can be orders of magnitude greater than the response due only to mechanical imbalance, particularly near rotor critical speeds. For the example considered, bent-shaft-moment excitation produces significantly higher response levels than the mechanical imbalance induced by thermal bow.

The impact of changes for (1) bearing length to diameter ratio, (2) reduced lubricant viscosity, (3) bearing radius-to-clearance ratio and (4) overhung mass magnitude are investigated. Reducing lubricant viscosity and/or the overhung mass are predicted to be the best remedies for Morton Effect problems.

## NOMENCLATURE

| | |
|---|---|
| $F, B$ | Forward and backward orbit amplitude |
| $L,R,D$ | Length, radius and diameter of bearing |
| $a, b$ | Semi major, minor elliptical orbit |
| $\alpha$ | Ellipse attitude angle |
| $\omega$ | Running Speed (rpm) |
| $C_r$ | Radial Clearance |
| $M_T$ | Bent shaft moment |
| $l_{gr}$ | Length between right bearing and mass center of right overhang |
| $m_{gr}$ | Mass of right overhang |
| $\beta_T$ | Thermal Bent shaft angle |
| $\Delta T_l$ | Effective maximum differential temperature |
| $\Delta T_f$, $\Delta T_b$, | Differential Temperature for forward and backward orbit |
| $\varepsilon_f$ , $\varepsilon_b$ | Ratio of forward and backward orbit to radial clearance |
| $\varphi_T$ | Location of effective hot spot wrt $x$ axis |
| $\varphi_{Tf}$, $\varphi_{Tb}$ | Phase angle between minimum film thickness and hot spot |

## INTRODUCTION

The Morton-Effect phenomenon is related to differential heating across a hydrodynamic bearing due to a synchronous orbit. When a journal is executing a synchronous orbit around an equilibrium position, one portion of the rotor surface is always at the minimum film thickness, while a diametrically opposite section of the journal surface is always at the maximum film thickness. Reduced film-thickness areas produce higher viscous shear stresses that produce higher temperatures. Larger clearances have reduced temperatures; hence, a temperature gradient develops across the journal, creating the slope $\beta_T$ across the journal (figure 1). For analysis, bent-shaft moments $M_T$,-$M_T$ can be applied at the bearing's ends to produce $\beta_T$. Synchronous rotor excitation from these moments are independent of running speed ω. Nicholas et al. [1] first examined the effect of residual shaft bow on the synchronous response of a single-mass rotor on a rigid support. Using a transfer-matrix approach, Salamone and Gunter [2] revisited shaft bow synchronous excitation for a multi-mass rotor in fluid-film bearing.

The rotor in figure 1 has an overhang, and the shaft bend $\beta_T$ is at the right-hand bearing. The overhung mass $m_{gr}$ has its mass center at the distance $l_{gr}$ to the right of the bearing's center. Hence, for small $\beta_T$ , the thermally induced mechanical imbalance is $m_{gr}l_{gr}\beta_T$.

The Morton Effect causes additional synchronous excitation in the form of (i) bent-shaft moments and (ii) thermally-induced mechanical imbalance. Large temperature gradients can induce high synchronous response. Sometimes, the response grows rapidly with increasing ω, leading to machine shutdown. Overhung compressors, integrally-geared compressors and double-ended drive turbines are specially impacted due to their heavy overhung mass properties [3].

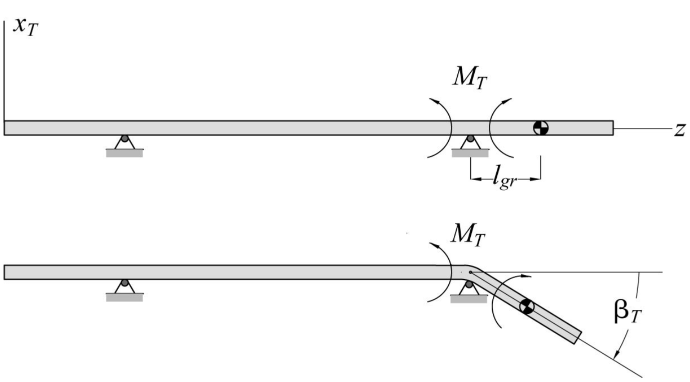


Figure 1. SHAFT WITH A THERMALLY-INDUCED BEND AT THE RIGHT-HAND BEARING

The Morton Effect was first observed by Paul Morton in the 1970s as spiral vibration behavior in generators with oil lubricated seals. Morton's early experimental investigations on the Morton Effect were published in internal company reports but were not available in the public domain. In 2008, Morton [4] provides a review of his earlier unpublished results including in-rotor temperature measurements. The results demonstrated a linear trend between orbit size and differential temperature. He found the in-rotor phase angle between the hot spot (point on the rotor where the temperature is a maximum) and the minimum film thickness location to be 60°. He reported a differential temperature of 16°C for an orbit size of 25% of the cold radial clearance.

In 1980, Kellenberger [5] analyzed spiral vibrations in oil lubricated, annular generator shaft seals assuming that the heat input to the shaft came from rubbing friction. In addition, he assumed that the ratio of the heat flow into the shaft to the heat flow out of the shaft determined the system stability; i.e., if this ratio was above some threshold curve, then the system would yield unstable spiral vibrations. Kellenberger's model worked well for spiral vibration problems due to rubbing.

In 1987, Schmied [6] investigated spiral vibrations due to hot spots on shafts and gave theoretical evidence of a change in rotordynamic behavior due to the bent shaft. He developed and solved a coupled eigenvalue problem of the rotordynamics plus thermal equation based on Kellenberger's model. He examined the heat input and the shaft vibration assuming , alternatively, that the heat input was proportional to: (i) shaft displacement, (ii) shaft velocity, and (iii) shaft acceleration. Schmied's model has bent shaft excitation, obtained by multiplying the rotor free-free stiffness matrix times the bent-shaft vector, consisting of the displacements and rotations of the shaft with the bent profile. He was the first person to propose spiral vibration as arising due to shearing of lubricant at a bearing. His hot-spot model was incorporated in the rotordynamics software MADYN, and has been applied for spiral vibrations problems due to rubbing or viscous shearing. He did not consider the effect of thermally-induced mechanical imbalance.

In 1993, Keogh and Morton [7] presented the first Morton-Effect analysis based on viscous heating of the lubricant within a plain journal bearing. The initial synchronous rotor excitation starts with an assumed bent shaft angle $\boldsymbol{\beta}_{0k}$ at a bearing that produces a bent shape for the rotor. Multiplying this shape by the rotor's free-free matrix produces a synchronous bent-shaft excitation, similar to Schmied's [6]. They decomposed the elliptic orbit at the bearing (figure 2) into circular orbits that are precessing, respectively, in the same direction as the rotor's spin direction (forward) and opposite to shaft rotation (backwards). Figure 3 shows this decomposition defined by

$$\begin{aligned} \boldsymbol{R}_0 &= \left(x_c \cos \omega t + x_s \sin \omega t\right) + \boldsymbol{j}\left(y_c \cos \omega t + y_s \sin \omega t\right) \\ &= F_0 e^{j(\omega t+\alpha)} + B_0 e^{-j(\omega t-\alpha)} = C_r \varepsilon_f e^{j(\omega t+\alpha)} + C_r \varepsilon_b e^{-j(\omega t-\alpha)} \end{aligned} \tag{1}$$

where, $C_r$ is the bearing's radial clearance, and $\varepsilon_f$ and $\varepsilon_b$ are respectively, the ratio of forward and backward precession orbits to $C_r$.

They used a short-bearing model with an iso-viscous lubricant to predict journal temperature distributions for a plain journal bearing with a coolant flow. They predicted that: (i) Forward and backward orbits produce separate (constant) rotor-fixed temperature distributions, and (ii) The backward precessing orbit also produces an oil film temperature distribution that precesses backwards at twice running speed, which can be ignored since the rotor temperature cannot respond to this high-frequency temperature oscillation. They assumed that the thermal bend development would be much slower than the rotordynamic response.

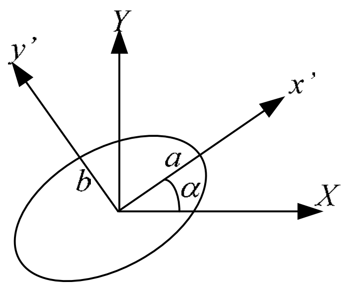


Figure 2. SYNCHRONOUS ELLIPTIC ORBIT FOR MOTION ABOUT AN EQUILIBRIUM POSITION

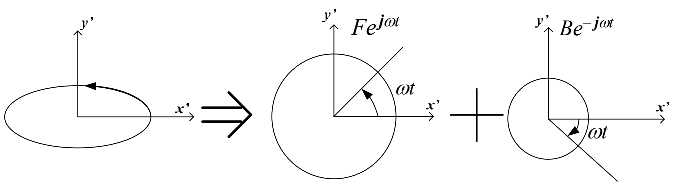


Figure 3. DECOMPOSING AN ELLIPTIC ORBIT INTO FORWARD AND BACKWARD CIRCULAR ORBITS.

Figure 4 shows the rotor-fixed *x,y,z* coordinate system. The angle $\varphi$ defines the circumferential location of a point on the rotor. For specified $\varepsilon_f$ and $\varepsilon_b$ values from Eq.(1), Keogh and Morton calculated the following rotor-fixed temperature distributions:

$$\Delta T_f\left(r,\varphi\right),\ \Delta T_b\left(r,\varphi\right) \tag{2}$$

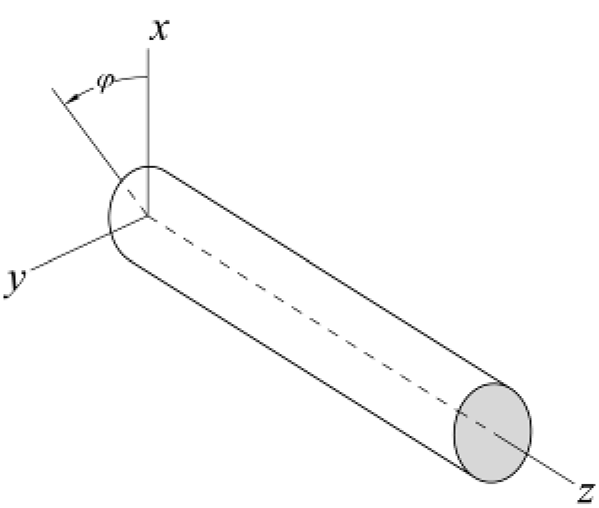


Figure 4. ROTOR-FIXED *x,y,z* COORDINATE SYSTEM

They assumed a linear radial temperature variation; i.e., $\Delta T_j\left(r,\varphi\right)=\Delta T_j,\ \Delta T_j\left(r,\varphi\pm\pi\right)=-\Delta T_j$, (where subscript *j* is either *f* or *b,* denoting a forward and backward orbit, respectively). They calculated a bent-shaft angle induced by the linear radial temperature gradient at the bearing using Dimoragonas' [8] closed-form solution

$$\begin{aligned}\boldsymbol{\beta}_{Tk} &= \beta_{Tx}+\boldsymbol{j}\beta_{Ty}\\ &=-\boldsymbol{j}\frac{\gamma_T}{I_a}\int_0^{2\pi}\int_0^{L}\int_0^{D/2}\Delta T_j\left(r,z,\varphi\right)\left(\frac{D}{2}\right)^2 e^{j\varphi}\,dr\,d\varphi\,dz\end{aligned} \tag{3}$$

where, $D$ and $L$ are the bearing's diameter and length, respectively. Further, $\gamma_T$ and $I_a$ are the coefficient of thermal expansion and area moment of inertia of the journal cross section, respectively.

As illustrated in figure 1, the hot side of the shaft is at the top of the rotor lying in the $x_T$ - $z$ plane. The cold side is at the bottom. The relative position of the *x, y* and $x_T$, $y_T$ axes is shown in figure 5 where the maximum differential temperature is located with respect to the *x* axis by $\varphi_T$.

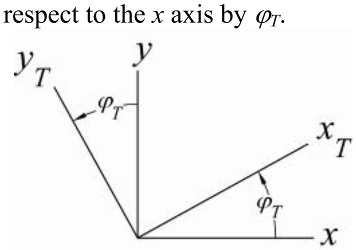


Figure 5. RELATIVE POSITIONS OF THE ROTOR FIXED *x,y,z* AND $x_T$,$y_T$,*z* COORDINATE SYSTEMS

Keogh and Morton expressed the net bend angle $\boldsymbol{\beta}_{Tk}=\boldsymbol{\beta}_{Tf}+\boldsymbol{\beta}_{Tb}$ where $\boldsymbol{\beta}_{Tf}$ is the forward, and $\boldsymbol{\beta}_{Tb}$ is the backward bent-angle component. Gain $\boldsymbol{G}_1$ is defined in terms of the ratio of temperature induced $\boldsymbol{\beta}_{Tk}$ and initial $\boldsymbol{\beta}_{0k}$ complex bent-shaft angles as

$$\boldsymbol{G}_1=\frac{\boldsymbol{\beta}_{Tk}}{\boldsymbol{\beta}_{0k}} \tag{4}$$

They suggest that Re($\boldsymbol{G}_1$)>1 indicates unstable growth, and Re($\boldsymbol{G}_1$)<1 indicates stable decay. Thermally-induced imbalance due to overhang was not considered.

In 1994, Keogh and Morton [9] developed a new analysis starting with time-varying bent-shaft angle components about the body-fixed *x* and *y* axes, instead of constant bent shaft angle. A time-dependent thermal bend was first calculated by combining the heat transfer equations with the dynamic equations of the rotor. This thermal bend was then transformed to the frequency domain where it was incorporated into a positive feedback loop. The stability characteristics of this loop were then obtained by plotting Nyquist graphs at successive rotor speeds. They obtained a range of instability speeds for which the real part of the eigenvalues were positive.

Geormiciaga and Keogh [10] used CFD techniques to analyze the dynamic flow and heat transport in the lubricant film in a hydrodynamic bearing and reported that the differential temperature generally increases with speed and orbit size.

In 1996, De Jongh and Morton [11] experimentally measured in-rotor temperatures at the tilting-pad bearing in a test rig to verify that the observed divergent synchronous vibration motion in a centrifugal compressor was caused by differential temperature across the journal. Their data are the only published in-rotor temperature measurements for hydrodynamic bearings. The experiments were done with a lightly-loaded rotor with a circular forward precessing orbit. They reported temperature difference of 3°C for the orbit size of 8% of the bearing clearance at 10500 rpm and an angle between the hot spot and position of minimum film thickness of 20°. They also found that repositioning the unbalance mass by an angle of 180° in the rotor resulted in a change of the location of the hot spot of about the same angle. The in-rotor temperature measurements shown in figure 6 was reported in subsequent publications by de Jongh and ver Hoeven [12]. However, the orbit amplitude, static eccentricity, running speed, and bearing specifications were not reported.

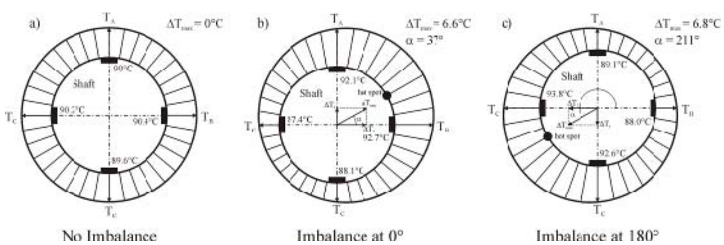

Figure 6. MEASURED IN-ROTOR TEMPERATURE [12]

De Jongh and Morton [11] developed an algorithm based on in-rotor temperature measurements to predict synchronous instability. Their rotor model is shown in figure 7, where $M_c$ is the concentrated overhung mass and $l$ is the distance between the overhung mass and the bearing. θ is the change in the bend angle due to differential temperature at the bearing location. The algorithm is based on the following three transfer functions (refer Figure 8): (1) $M_c l$ (overhung moment at the bearing), (2) $\boldsymbol{I_{OB}}$ ("influence coefficient between the overhung and the bearing location") and depends on ω, the mode shape, system damping and proximity to critical speed, and (3) $\boldsymbol{T}(t,\omega)$ (complex thermal gain) is a function ω and time t to be obtained from experimental measurements. The scheme established (shown in Figure 8) defines $\boldsymbol{G}$ as the product of three transfer functions. They state that Re($\boldsymbol{G}$) should be less than 1 for Morton-Effect rotor stability.

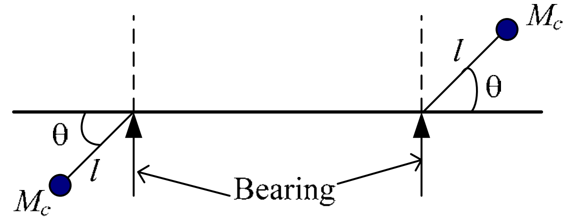

Figure 7. OVERHANG MODEL BY DE JONGH AND MORTON [11]

In 2000, Balbahadur and Kirk [13] developed a theoretical model for Morton-Effect analysis. The bearing's circumferential temperature distribution was determined by solving the thermal energy balance equation based on the heat generation rates occurring between the journal, lubricant, and bearing. The temperature distribution is used to calculate the thermally-induced mechanical imbalance. The net imbalance is calculated as a vector sum of mechanical imbalance (taken as 10% of total weight of rotor divided by $\omega^2$) and the thermally induced mechanical imbalance. For stability, they state that the net imbalance should be less than the threshold imbalance (15% of the total rotor weight divided by $\omega^2$). The hot spot is assumed to coincide with the minimum film-thickness location, contradicting experimental observations by Morton [4] and De Jongh and Morton [11], plus predictions by Geomiciaga and Keogh [10]. Balbahadur and Kirk validate their approach by comparing their predictions to observed outcomes for multiple case studies [14]. They did not consider induced bent-shaft excitation or separate contributions due to forward and backward orbits.

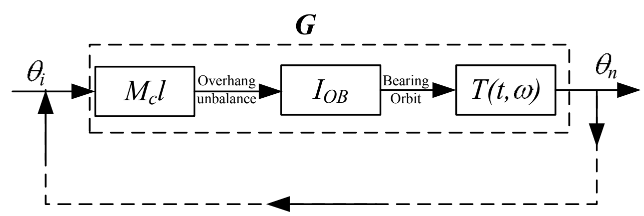

Figure 8. SCHEME OF INSTABILITY PHENOMENON AFTER [11]

Murphy and Lorenz [15] presented a simplified method for modeling the Morton Effect. They used the following vectors: (1) $\boldsymbol{A}$ (sensitivity of vibration due to mechanical imbalance), (2) $\boldsymbol{B}$ (temperature coefficient vector connecting hot spot on the shaft and position of minimum film thickness), and (3) $\boldsymbol{C}$ (bow coefficient vector, connecting the imbalance vector and the hot spot). For stability, they argue that Re($\boldsymbol{ABC}$) should be less than 1. The temperature difference is found to be linearly proportional to the size of the shaft orbit, and they calculated the orbit due to Morton Effect. The temperature profile of the lubricant used for the analysis is obtained by a separate CFD calculation.

Multiple case studies exist for machines that have encountered divergent synchronous motion, and de Jongh [16] provides an excellent literature overview and review of corrective measures for the Morton Effect.

## RESEARCH OBJECTIVE

A review of existing analysis techniques shows that the Morton-Effect response has, until now, been considered as a classical stability problem to be resolved by eigenanalysis or a related stability technique. In general, linear stability analyses consider the stability of motion resulting from a perturbation from an equilibrium point or orbit. However, existing techniques seem to omit the initial step of finding an equilibrium orbit. The present analysis aims to iteratively construct equilibrium orbits, starting from synchronous response due to an initial mechanical imbalance distribution, and then considering the additional excitation due to a thermally-induced bent-shaft and a thermally-induced mechanical imbalance. The analysis leaves open the question of whether the resultant equilibrium orbits are stable.

## ALGORITHM DEVELOPMENT

The algorithm is motivated by the 1993 Keogh and Morton paper [7]. It starts with calculated synchronous response results for an initially specified imbalance distribution that, for each running speed ω, produces a static eccentricity ratio $\varepsilon_0$ and an attitude angle $\psi_0$ at a bearing. For this equilibrium position, the contents of Table 1 are calculated by solving the Reynolds equation plus the energy equation. The predictions in Table 1 are calculated differential temperature and phase lag angles for a plain journal bearing for forward and backward orbits at ω=7500 rpm for $\varepsilon_0$=0.667, $\psi_0$=41.2$^0$, $L$=35*mm*, $D$=100*mm*, $C_r$=100$\mu m$, $\mu$ (absolute viscosity) = 0.08 *Pa-s*. The phase-angles of Table are illustrated in Figure 9 and define the locations of hot spots for forward and backward orbits from the minimum-film thickness location.

The bearing-temperature-solution algorithm leading to the contents of Table 1 is similar to that of Keogh and Morton [7] but is based on the work of Gadangi et al. [17] and was produced using a model and code developed under the leadership of Professor Alan Palazzolo at Texas A&M University. Calculating these and similar results takes an order-of-magnitude more time than the synchronous Morton-Effect calculations.

Table 1. CALCULATED DIFFERENTIAL TEMPERATURE AND PHASE LAG ANGLES FOR FORWARD AND BACKWARD ORBIT

| $\frac{F}{C_r}$ | $\Delta T_f$ (°C) | $\varphi_{Tf}$ | $\frac{B}{C_r}$ | $\Delta T_b$ (°C) | $\varphi_{Tb}$ |
|---|---|---|---|---|---|
| 0.05 | 0.7361 | 72 | 0.05 | 0.7898 | -84 |
| 0.10 | 0.9314 | 36 | 0.10 | 0.9058 | -48 |
| 0.20 | 2.0425 | 24 | 0.20 | 2.1279 | -24 |
| 0.25 | 8.5327 | 12 | 0.25 | 7.8965 | -12 |
| 0.30 | 13.785 | 36 | 0.30 | 12.6534 | -54 |

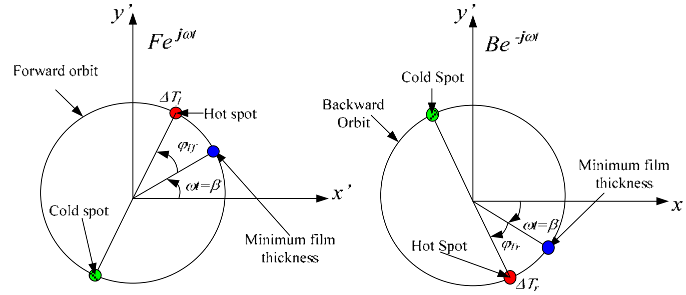


Figure 9. MAXIMUM DIFFERENTIAL TEMPERATURE AND PHASE LAG ANGLES FOR FORWARD AND BACKWARD ORBITS

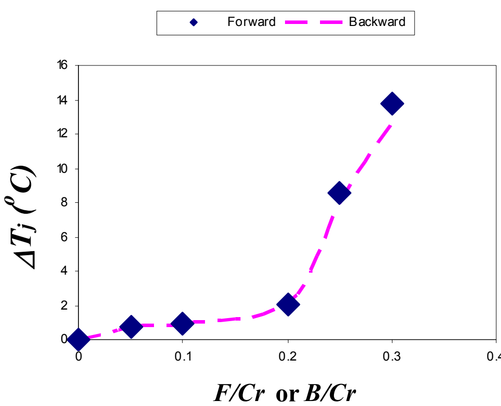


**(a)**

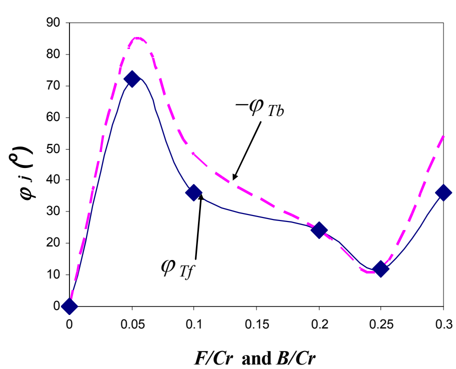


**(b)**

Figure 10. (A) CALCULATED $\Delta T_f$,$\Delta T_b$ AND (b) $\varphi_{Tf}$,$\varphi_{Tb}$ VERSUS ORBIT AMPLITUDE AT 7500 RPM AT $\varepsilon_0$=0.667 FROM TABLE-1

Figures 10(a) and (b) illustrate predictions of $\Delta T_j$ and $\varphi_{Tj}$ from Table 1 for a range of forward and backward orbit amplitudes. For $F/C_r$ and $B/C_r$ up to ~0.2 $\Delta T_j$ behaves linearly, but as the orbit size increases, the behavior becomes nonlinear. The $\Delta T_j$ increase rapidly as $\varepsilon_0$+ $F/C_r$ approaches 1; i.e., motion approaching the clearance.

We are only going to discuss the Morton-Effcet algorithm for the right bearing of figure 1 although the procedure applies for an overhang at either or both bearings. Proceeding with the algorithm, the initially calculated synchronous response at the right bearing is an elliptical orbit that produces forward and backward orbit radii $F_0$ and $B_0$. Using $F_0/C_r$ and $B_0/C_r$ as input, $\Delta T_f$, $\Delta T_b$, $\varphi_{Tf}$ and $\varphi_{Tb}$ are obtained by interpolation from Table 1. Hence, the net rotor-fixed temperature distribution is

$$\Delta T_1 e^{j\varphi_T} = \left(\Delta T_f \cos\left(\beta^* + \varphi_{Tf}\right) + \Delta T_b \cos\left(\beta^* + \varphi_{Tb}\right)\right) + \boldsymbol{j}\left(\Delta T_f \sin\left(\beta^* + \varphi_{Tf}\right) - \Delta T_b \sin\left(\beta^* + \varphi_{Tb}\right)\right) \quad (5)$$

The resultant maximum differential temperature $\Delta T_1$ and its location $\varphi_T$ with respect to the $x$ axis is

$$\Delta T_1 = \sqrt{\Delta T_f^2 + \Delta T_b^2 + 2\Delta T_f \Delta T_b \cos\left(2\beta^* + \varphi_{Tf} + \varphi_{Tb}\right)}$$
$$\varphi_T = \tan^{-1}\left(\frac{\Delta T_f \sin\left(\beta^* + \varphi_{Tf}\right) - \Delta T_b \sin\left(\beta^* + \varphi_{Tb}\right)}{\Delta T_f \cos\left(\beta^* + \varphi_{Tf}\right) + \Delta T_b \cos\left(\beta^* + \varphi_{Tb}\right)}\right) \quad (6)$$

From Dimoragonas [8], the resultant bent angle $\beta_T$ is

$$\beta_T = \Delta T_1 \frac{\pi \gamma_T}{4 I_a} L \left(\frac{D}{2}\right)^3 \quad (7)$$

An applied moment $M$ at the end of a cantilevered Euler beam produces the rotation angle $\beta = ML / EI_a$. Hence, $\beta_T$ is produced by the following end moment

$$\beta_T = M_T L / EI_a \Rightarrow M_T = \frac{\pi}{4}\left(\frac{D}{2}\right)^3 E \gamma_T \Delta T_1 \quad (8)$$

Observe that $M_T$ is not a function of $L$. Applying $M_T$ and $-M_T$ moments at the right and left hand ends of the bearing produces $\beta_T$. The signs of $M_T$ and $-M_T$ correspond to right-hand rotation directions about the $y_T$ axis. With respect to the rotor model, $M_T$ and $-M_T$ are applied at stations $i^*$ and $j^*$ corresponding to the station on the left and right hand end of the right bearing, respectively. *The synchronous response due to this bent-shaft excitation is calculated as the first additional contribution to the synchronous response.* This excitation is applied directly to the rotor model versus using the rotor free-free matrix as carried out by other methods.

The portion of the rotor outside the right-hand side bearing has mass $m_{rb}$, and its mass center lies the distance $l_{gr}$ to the right of the bearing center at station $k^*$ in the rotor model. For small $\beta_T$, a thermally-induced mechanical imbalance occurs with the magnitude $m_{rb} l_{gr} \beta_T$. *The synchronous response due to this thermally-induced imbalance is calculated as the second additional contribution to the synchronous response.*

The three synchronous responses are added vectorially (response due to initial mechanical imbalance + response due to bent-shaft excitation + response due to thermally-induced imbalance) producing a new starting ellipse, and the process is continued until a converged orbit is produced.

At the end of each iteration step, the gain factor

$$G_{aT} = \frac{F_i + B_i}{F_{i-1} + B_{i-1}} \quad (9)$$

is calculated where, $F_i$ and $B_i$ are forward and backward amplitudes, respectively at the end of $i^{th}$ iteration. $G_{aT}$ is a real number, not complex. ($G_{aT}$ *-1)* is checked to see if it is less than tolerance (0.001 for the present calculations); if yes, the steady state converged solution is obtained. Otherwise, the iteration continues for a set number of cycles. *For the cases considered here and discussed below, the algorithm continues to converge until motion approaches the wall.* Convergence problems can arise in the form of oscillations if the interpolation grid presented by Table 1 is too coarse.

## Keogh and Morton's (1994) Symmetric Rotor Example [9]

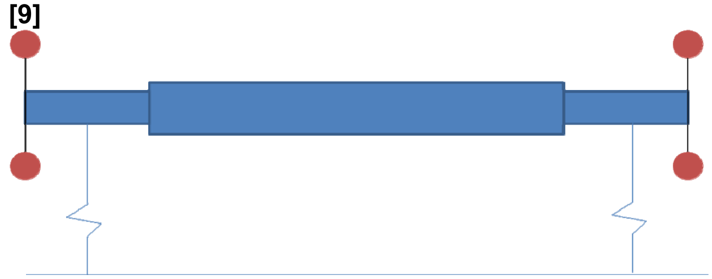

Figure 11. ROTORDYNAMIC MODEL OF KEOGH AND MORTON [9], SYMMETRIC ROTOR

Figure 11 shows a symmetric flexible rotor with end-mounted discs (each with mass 20 kg), supported by two identical plain journal bearings. The bearings are at stations 5 and 41, with $L$=35 *mm*, $D$=100 *mm*, $C_r$=100 $\mu m$ and $\gamma_T$=1.1e$^{-5}$/$^0$C. The bearing's calculated $\varepsilon_0$, $\psi_0$, and $\mu$ versus ω are given by [11]. Because $L/D$ = 0.35, the short-bearing model [18] is used to calculate rotordynamics coefficients. The rotor's first and second critical speeds are ~4000 and ~7000 rpm, respectively. The first forward damped mode is a cylindrical rigid-body mode. Assuming, the maximum continuous operating speed is 6000 rpm; the API 684 [3] imbalance is set at ~50 *gm-cm* and is applied at the rotor's mid-span. This imbalance excitation provides minimal excitation for the 2$^{nd}$ mode.

In the following discussion, "Morton Effect" means that additional synchronous response contributions are calculated including contributions from the thermally-induced bent-shaft excitation and the thermally-induced mechanical imbalance. Figure 12 presents $\rho_{max}$ versus ω for the original model with Morton Effect where $\rho_{max}$ is the normalized relative rotor displacement using radial clearance from the bearing center. $\rho_{max}$ cannot exceed unity without contact. At speeds beyond 10000 rpm, $\rho_{max}$ exceeds the clearance circle, i.e., the response diverges. Below this speed, steady-state converged solutions are obtained. The distinct peaks at 4000 and 7000 rpm are at the 1st and 2nd critical speeds. Obviously, operation near a critical speed can produce higher levels of synchronous vibration. Near a critical speed, the higher amplitudes result in higher $\Delta T$s, which causes higher synchronous excitation due to Morton Effect.

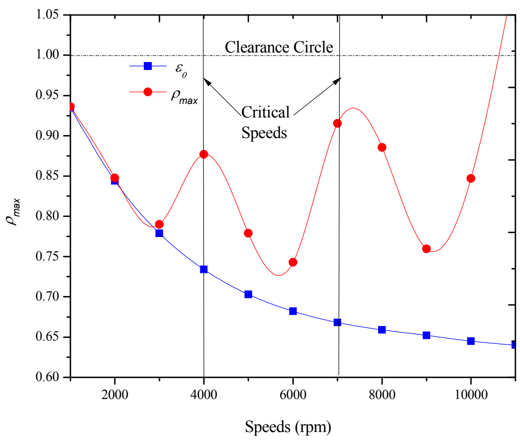


Figure 12. MORTON EFFECT RESPONSE $\rho_{max}$ VERSUS ω OF ORIGINAL MODEL

Keogh and Morton [9] calculated an instability zone between 9769 rpm and 10371 rpm. Balbahadur and Kirk [14] predicted the resultant imbalance exceeding threshold imbalance between 10001 rpm to 11521 rpm. The present algorithm predicts diverging motion at speeds above ~11000 rpm and does not predict recovery at higher speeds. De Jongh and Morton [11] observed recovery in Morton Effect instability at higher speeds.

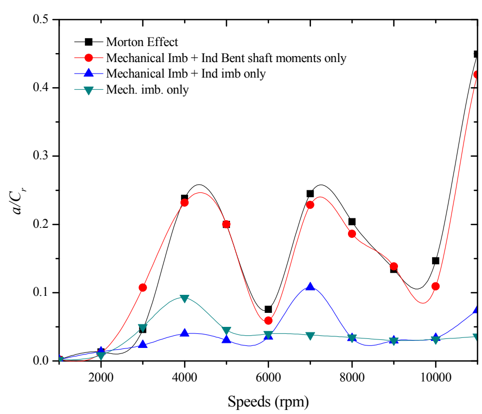


Figure 13. $a/C_r$ VERSUS ω WITH FOR VARIOUS COMBINATIONS OF MORTON EFFECT

Figure 13 presents $a/C_r$ ($a$ is the semi-major axis of the ellipse) versus ω for: (i) Mechanical imbalance only, (ii) Morton Effect, (iii) Mechanical imbalance + thermally-induced bent-shaft excitation, and (iv) Mechanical Imbalance + thermally-induced imbalance. For this case the thermally-induced bent-shaft excitation is the dominant contributor to the response. However, this dominant outcome is not certain, since the overhung mass can be increased, increasing the induced imbalance without changing the bent-shaft excitation. The response diverges (again) at ~11000 rpm.

## IMPACT OF INCREASING INITIAL IMBALANCE

Figure 14 shows significant increases in the Morton synchronous response when the mechanical imbalance magnitude is increased from 50 *gm cm* to 100*gm cm*. The divergent speed drops to 7000 rpm from 110000 rpm. The larger mechanical imbalance causes a larger orbit amplitude that drives the larger differential temperature in the bearing, which in turn provides higher synchronous excitations due to Morton Effect. Recall that the algorithm requires some initial mechanical imbalance to obtain an orbit to begin iterative calculations.

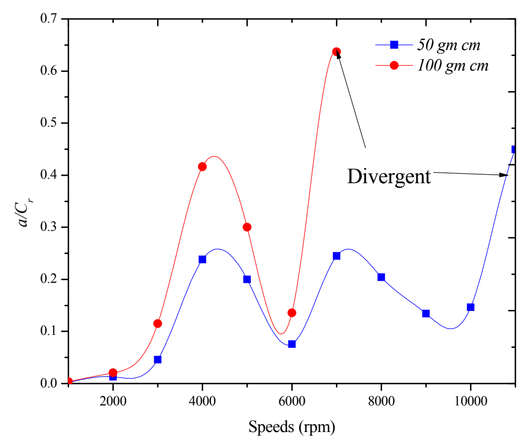


Figure 14. MORTON EFFECT SYNCHRONOUS RESPONSE WITH CENTERED IMBALANCES OF 50 *gm cm* AND 100 *gm cm*

## IMPACT OF CHANGING *L/D*

Figure 15 presents $\rho_{max}$ versus ω for $L/D$= 0.35 and $L/D$= 0.5. For $L/D=0.5$, $\rho_{max}$ does not cross the clearance circle for speeds up to 11000 rpm, indicating no divergent motion . $\varepsilon_0$ is smaller with $L/D=0.5$ than *0.35* , as increasing $L/D$ reduces the bearing unit load. Increasing $L/D$ is predicted to reduce the synchronous response due to Morton Effect. The predictions of figure 14 conflicts with some experiences. Berot and Dourlens [19] and Schmeid et al.[20] eliminated Morton Effect instability problem by reducing $L/D$ for tilting-pad bearing. Schmeid et al. state, "the thermal deflection per unit temperature rise in the bearing cross section is proportional to the width of bearing". For both configurations in figure 15, $\varepsilon_0$~0.4-0.7 in contrast of the turbo-expander model discussed by Schmeid et al. that have $\varepsilon_0$~0.05. Figure 16 predicts that increasing $L/D$ decreases $\Delta T$, which explains the difference in the synchronous response. An extension of the new algorithm to include an analysis of orbit stability might show that orbits associated with small L/D ratios are more stable than orbits associated with large L/D ratios.

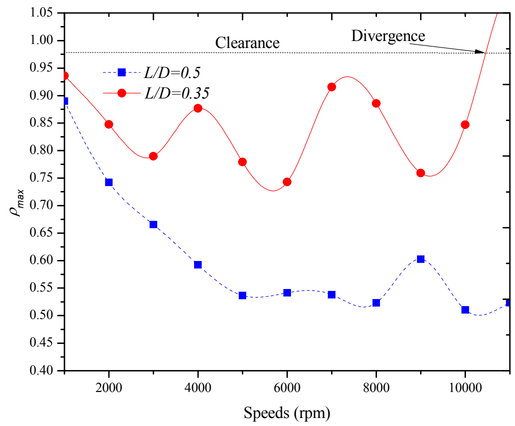


Figure 15. MORTON EFFECT RESPONSE-$\rho_{max}$ VERSUS $\omega$ FOR DIFFERENT *L/D* RATIOS

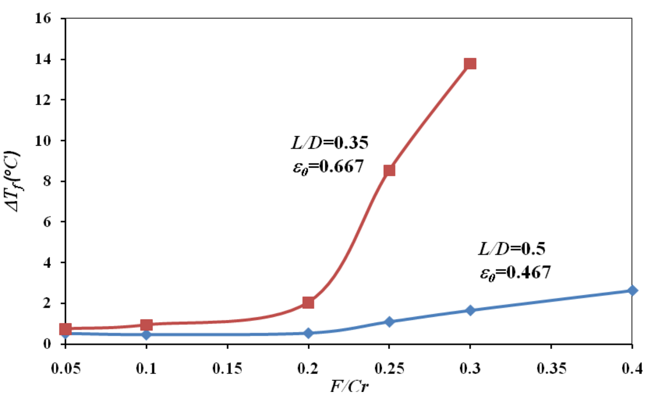


Figure 16. $\Delta T_f$ VERSUS *F/Cr* FOR *L/D=0.35* AND *0.5* AT 7500 rpm

## IMPACT OF CHANGING $C_r/R$

This section examines the predicted influence of changing $C_r/R$ from 0.002 to 0.001. The predicted differential temperature and phase angles for different $\varepsilon_0$, $\psi_0$, and $\mu$ values at different speeds is given in Saha [21]. Reducing the clearances, reduces the operating eccentricity but increases the differential heating. The power dissipated by a centered plain journal bearing is inversely proportional to $C_r$ [22].

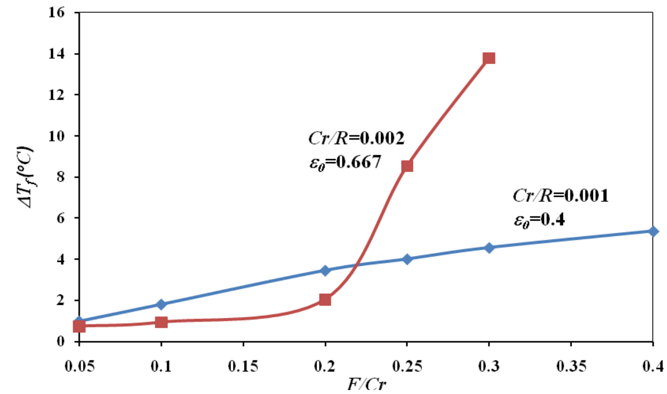


Figure 17. $\Delta T_f$ VERSUS *F/Cr* FOR *Cr/R=0.001* AND *0.002* AT 7500 rpm

Figure 17 shows the differential temperature increasing by an approximate factor of 2 for $C_r/R$=0.001 as compared to $C_r/R$=0.002. $\Delta T_f$ increases more or less linearly for $C_r/R$=0.001 For $C_r/R$=0.002, it first rise linearly up to *F/Cr*=0.2; beyond that it rise sharply with increasing $F/C_r$. As the orbit amplitude approaches the clearance, higher shear viscous forces and larger differential temperature result.

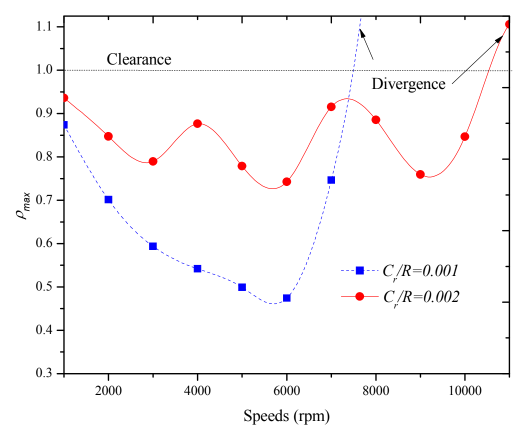


Figure 18. MORTON EFFECT RESPONSE $\rho_{max}$ VERSUS $\omega$ FOR DIFFERENT *Cr/R* RATIOS

Figure 18 predicts that reducing $C_r/R$ from 0.002 to 0.001 causes the system to diverge due to the Morton Effect above 7000 rpm. No recovery in response is predicted with increasing ω.

Deliberately increasing $C_r$ has not been considered as an option to fix Morton Effect problems; however, de Jongh and van der Hoeven [12] noted that there compressor was subject to the Morton Effect Instabilities in the field because reduced ambient temperatures reduced the clearances.

## INFLUENCE OF OVERHUNG MASS MAGNITUDES

Figure 19 compares $\rho_{max}$ versus ω for the original model with an overhung mass of 20 kg and a modified model with 50 kg. Saha[21] tabulated the predicted differential temperature and phase angles for different $\varepsilon_0$, $\psi_0$, and $\mu$ values at different speeds. Increasing the magnitude of the overhung mass, increases the operating eccentricity and consequently increases the differential heating. The thermally-induced mechanical imbalance is directly proportional to the product of the overhung mass and its distance from the bearing. The 50kg mass is predicted to cause a sharp rise in response after 3000 rpm making the response diverge. This prediction confirms the general field experience that reducing the overhung mass magnitude helps to eliminate Morton Effect problems. Corcoran et al. [23] present the only contrary result where a significant increase in coupling weight eliminated a Morton-Effect problem.

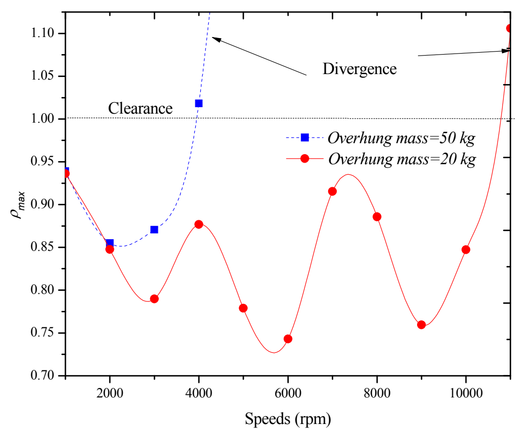


Figure 19. MORTON EFFECT RESPONSE $\rho_{max}$ VERSUS ω FOR DIFFERENT OVERHANG MASSES

## INFLUENCE OF REDUCED LUBRICANT VISCOSITY

This model has 70% of the original viscosity by Keogh and Morton [9]. The remaining parameters are the same. Saha[21] provides the predicted differential temperature and phase angles for different $\varepsilon_0$, $\psi_0$, and $\mu$ values at different speeds for the reduced viscosity. Reducing viscosity increases the operating eccentricity, but reduces the differential heating. Figure 20 presents $\rho_{max}$ versus ω for the Morton Effect with the original and reduced viscosity. No divergent motion is predicted for reduced viscosity for ω out to 12k rpm. Schmeid et al. [20] and Marscher and Illis [24] (increased the supply temperature) reduce viscosity to eliminate Morton Effect problems.

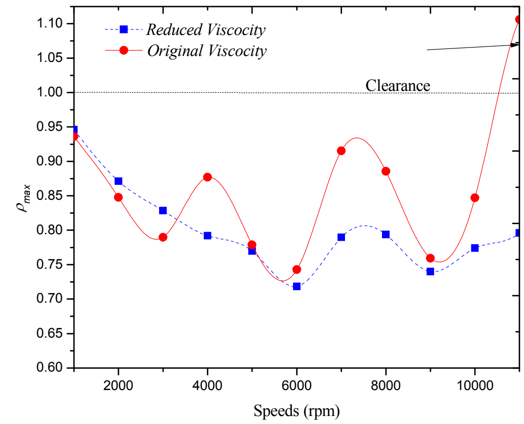


Figure 20. MORTON EFFECT RESPONSE $\rho_{max}$ VERSUS ω FOR DIFFERENT VISCOSITIES

## SUMMARY, CONCLUSIONS, AND DISCUSSION

The approach and results presented here provide an alternative viewpoint for analyzing the Morton Effect phenomenon. Specifically, an iterative approach is used to produce a converged orbit for the rotor versus attempting to ask whether a rotor is "stable" or unstable under the influence of Morton Effect differential heating at the bearing. For the cases considered, the algorithm produced a converged orbit for all cases until motion approaches the bearing wall; i.e., cases in which contact is predicted. The speeds for which contact is predicted agree reasonably well with predictions from prior stability approaches.

In contrast to some stability algorithms, the present approach did not predict higher-speed "recovery" ranges for which the Morton Effect phenomenon disappeared. De Jongh and Morton [11] observed this outcome in tests, but did not cite corresponding predictions of recovery.

The new model's results also differs from prior analyses in predicting substantial differences in synchronous response due to the Morton effect during critical-speed transitions well before speeds that cause divergent motion. De Jongh and Morton's measurements confirm these predictions [11].

Predictions from the algorithm are generally consistent with experiences except in regard to the impact of changing *L/D*. For the example considered, the present model predicted an improvement with increasing *L/D*; whereas, several case studies have been presented that show an opposite outcome. As yet, no attempt has been made to investigate the stability of the converged orbital solutions presented here. Field experiences in which the rotor phase changes continuously at constant speed clearly argue that some of the observed orbits are unstable. A more complete model of the rotor and bearing would be needed to conduct a stability analysis. Further stability analysis might show that orbits with reduced *L/D* values are more dynamically stable. Note also that calculated results from all algorithms have been for plain journal bearings while most operating experiences have been with tilting-pad bearings.

However, the reverse side of this statement is that prior stability analyses have failed to start from an equilibrium orbit in performing stability analyses. In the related phenomenon of spiral vibrations due to rub, motion is dynamically unstable for small motion about many initial starting points. However, the resultant motion can proceed to either a stable orbit or an unstable orbit [5], [8].

The code based on the iterative algorithm presented here runs very quickly. However, that speed is deceptive since the code that is required to produce the results of Table 1 require about 6-8 hours of execution time for one point (one forward or one backward orbit) for a plain journal bearing with constant viscosity. Assuming that one produces predictions at multiple speeds and multiple orbit amplitudes, many hours of computer time are required. Predictions are becoming available for variable viscosity, and progress is being made for tilting-pad bearings.

The real deficit in regard to the Morton Effect is the almost complete absence of in-rotor temperature measurements to validate any existing theory or approach. Most companies have developed approaches to "manage" the problem with the present inadequate knowledge base, so there is no greater incentive to spend money to get a better understanding.

Saha [21] provides an extended discussion of the algorithm including comparative calculated results for the model of Schmied et al. [20].

## REFERENCES


[1] Nicholas, J. Gunter, E., and P. Allaire, 1976, "Effect of residual shaft bow on unbalance response and balancing of a single mass flexible rotor, Part 1: Unbalance response," ASME J. Eng. for Power, **98**(2), pp.171-181.

[2] Salamone, D., and Gunter, E., 1978, "Effects of shaft warp and disk skew on the synchronous unbalance response of a multimass rotor in fluid film bearings," *Proc. of ASME fluid film bearing and rotor bearing system design and optimization*, pp.79-107.

[3] API 684 Standard, 2005, "*API Standard Paragraphs Rotordynamic Tutorial: Lateral Critical Speeds, Unbalance Response, Stability, Train Torsionals, And Rotor Balancing*," Tech. Rep., Washington DC.

[4] Morton, P., 2008, "Unstable shaft vibrations arising from thermal effects due to oil shearing between stationary and rotating elements," *IMECHE Proc. of International Conference on Vibrations in Rotating Machinery*, Exeter, England.

[5] Kellenberger, W., 1980, "Spiral vibrations due to the seal rings in turbogenerators thermally induced interaction between rotor and stator," ASME J. of Mech. Design, **102**(1), pp. 177-184.

[6] Schmied, J., 1987, "Spiral Vibrations of Rotors," *Proc. of 11th Biennal ASME Design Engineering Div. Conference, Vibration and Noise, Rotating Machinery Dynamics*, Boston, MA, pp. 449-456.

[7] Keogh, P., and P. Morton, 1993, "Journal Bearing Differential Heating Evaluation with Influence on Rotor Dynamic Behaviour," Proc. of Royal Soc. London, Series A: Math. Phys. Sci., **441**(1913), pp. 527-548.

[8] Dimorgonas, A., 1970, "Packing Rub Effect in Rotating Machinery," Ph.D. Dissertation, RPI, Troy, NY.

[9] Keogh, P., and P. Morton, 1994, "Dynamic Nature of Rotor Thermal Bending due to Unsteady Lubricant Shearing within a Bearing," Proc. of Royal Soc. London, Series A: Math. Phys. Sci. **445**(1924), pp. 273-290.

[10] Gomiciaga, R., and P. Keogh, 1999, "Orbit induced J. temperature variation in hydrodynamic bearings," J. Trib., **121**(1), pp. 77-84.

[11] De Jongh, F., and P. Morton, 1996, "The Synchronous Instability of a Compressor Rotor due to Bearing Journal Differential Heating," J. of Eng. for Gas Turbines and Power, **118**(4), pp. 816-822.

[12] De Jongh, F., and P. van der Hoeven, 1998, "Application of Heat Sleeve Barrier to Synchronous Rotor Instability," *Proc. of 27th Turbomachinery Symposium*, Houston, TX, Turbomachinery Laboratory, College Station, TX.

[13] Balbahadur, A., and R. Kirk, 2004, "Part 1-theoretical model for a synchronous thermal instability operating in overhung rotors," Int. J. Rotating Mach., **10**(6), pp. 469-475.

[14] Balbahadur, A., and R. Kirk, 2004, "Part 2-case studies for a synchronous thermal instability operating in overhung rotors," Int. J. Rotating Mach., **10**(6), pp. 477-487.

[15] Murphy, B., and J. Lorenz, 2009, "Simplified Morton Effect Analysis for Synchronous Spiral Instability," *Proc. of PWR2009*, pp. 21-23, Albuquerque, NM.

[16] De Jongh, F. M., 2008, "The Synchronous Rotor Instability Phenomenon --- Morton Effect," *Proc. of 27th Turbomachinery Symposium*, Houston, Tx, Texas A&M University, Turbomachinery Laboratory, College Station, TX.

[17] Gadangi R. K., Palazzolo A. B., Kim J., 1996, "Transient Analysis of Plain and Tilt Pad Journal Bearings Including Fluid Film Temperature Effects"ASME J. Tribol. **118** (2), pp.423-430.

[18] Lund, J. W., 1966, "Self-Excited, Stationary Whirl Orbits of a Journal in a Sleeve Bearing," Ph.D. Dissertation, RPI, Troy, NY.

[19] Berot, F., and H. Dourlens, 2000, "On Instability of Overhung Centrifugal Compressors," *Proc. of ASME IGTI Turboexpo 2000*, Indianapolis, IN.

[20] Schmied, J., Pozivil, J., and J. Walch, 2008, "Hot Spots in Turboexpander Bearings: Case History, Stability Analysis, Measurements and Operational Experience," *Proc. of ASME IGTI Turboexpo 2008,* Berlin, Germany.

[21] Saha, R., 2010, A New, Iterative, Synchronous Response Algorithm for Analyzing Morton Effect, Master's Thesis, College Station, TX.


 

[22] Pinkus, O., and Sternlicht, B., 1961, "*Theory of Hydrodynamic Lubrication*", 2nd Edition, McGraw Hill, New York.

[23] Corcoran, J., Rea, H., Cornejo, G., and M. Leonhard, M., 1997, "Discovering, the Hard Way, How a High Performance Coupling Influenced the Critical Speeds and Bearing Loading of an Overhung Radial Compressor—A Case History ," *Proc. of 17th Turbomachinery Symposium*, College Station, TX.

[24] Marscher, W. D., and B. Illis, 2007, "J. Bearing Morton Effect Cause of Cyclic Vibration in Compressors," Trib. Trans., **50**(1), pp. 104-113.